Supplementary Information

Calcite-functionalized microfluidic chip for pore scale investigation of biogeochemical interactions in porous media

Na Liu*[a] and Martin A. Fernø [a, b]

[a] Department of Physics and Technology, University of Bergen, Norway.

[b] Norwegian Research Centre AS – NORCE, Norway.

*Corresponding author: Na Liu, Na.Liu@uib.no

Material & Methods

Experimental setup

The micromodel with chip holder was imaged using a Zeiss Axio Zoom V16 microscope with a cold-light (CL 9000 LED) and fluorescent light source, which provide a resolution of 4.38 µm/pixel. This setup (**Figure S1**) captured microbial activity, fluid flow and $CaCO_3$ precipitation processes across the pore network [1, 2]. Temperature was maintained at constant by circulating warm water through copper tubes in the chip holder. Pressure was precisely controlled using a high-precision plunger pump (Quizix Q5000-10K) and a back pressure regulator (EB1ZF1 Equilibar Zero Flow). The plunger pump operates in either constant injection rate or constant injection pressure mode, delivering liquid and gas into the micromodel at precise flow rates (0.03 µL/min – 15 mL/min) and desired pressures (0-120 barg). Absolute pressure readings were obtained from two ESI APLISENS PRE-28 SMART transmitters (0–2.5 barg range, with a static limit of 250 barg), which were mounted on the flow ports. The experimental setup has a high-precision injection system with a constant dead-volume (10 µL), including a two-position switch valve (Idex, 9725) and two 6-ports select valves (Idex, MXP7970-000). The experimental setup features a high-precision injection system with a constant dead volume (10 µL), comprising a two-position switch valve (Idex, 9725) and two 6-port select valves (Idex, MXP7970-000). Prior to each experiment, the system was cleaned with ethanol, deionized water, and H_2O_2, followed by flushing with >100 pore volumes of DI water. Bypass lines facilitated cleaning of the tubing and prevented mixing and reactions before the solution entered the pore network. Further details on the experimental setup can be found in our earlier publications [3, 4].

Experimental procedure for microbial-induced $CaCO_3$ precipitation (MICP) process

The bacterial solution was prepared by mixing 0.2 mL of a dense bacterial suspension (10^9 cells/mL) with 10 mL of a nutrient solution containing 4.7 wt.% brain heart infusion broth and 2 wt.% urea (pH ≈ 7.41). This mixture was incubated overnight at 30°C. Prior to inoculation, the micromodel was pre-cleaned with ethanol, deionized water, and H_2O_2, followed by flushing with >100 pore volumes (PVs) of deionized water. To flush residual water from the pore network, 20 PVs of nutrient solution were injected. Then, 10 PVs of the bacterial solution (OD600 = 0.89, ~7×10^8 cells/mL, pH = 9.51) were injected into the micromodel at 30°C. After 16 hours for bacterial attachment, 1.5 PVs of cement solution (0.5 M $CaCl_2$ + 0.5 M Urea) were injected into the pore network at 1 µL/min to precipitate calcium carbonate. The distribution of the precipitates was visualized using the high-resolution microscope. After a single cycle of MICP treatment, the injection tube became clogged with

precipitates. To resolve this, the chip will be removed from the stage and submerged in a weak acid solution (0.1 M HCl) for 1 hour to clear the inlet. The MICP process can be repeated multiple times until the desired porosity is achieved.

Raman spectroscopy test

To analyze $CaCO_3$ precipitates in the micromodel at different stages, a Horiba LabRam HR confocal Raman spectrometer with a 488 nm argon laser was used to capture Raman shifts from 200 to 1600 cm^{-1}. After the carbonate precipitates formed in the pore network, the micromodel was depressurized to ambient conditions and disconnected from the experimental setup. The precipitates were then analyzed in situ to identify $CaCO_3$ polymorphs at a 2 µm spatial resolution.

Image acquisition and segmentation

After $CaCO_3$ precipitates formed in the pore network, images were consistently captured in fluorescence (blue channel) and brightfield modes. Acquiring 121 images of the entire network took 277 seconds, with continuous imaging during crystal nucleation and growth. An in-house coded Python algorithm was used for image segmentation and analysis. Both channels were converted to grayscale to compute their respective histograms. Pore space was segmented from silicon grains in the brightfield images using OpenCV thresholding, while $CaCO_3$ precipitates appeared brown due to dye from the fluorescent salt and were identified through color extraction. The fluorescence channel was segmented into two classes—the silicon-$CaCO_3$ phase and water phase—using the Multi-Otsu algorithm from the scikit-image library . Porosity was quantified by summing pore space pixels and dividing by the total image size. Porosity reduction was calculated as the ratio of $CaCO_3$ precipitates pixels to total pore space. Only fully depth-saturated $CaCO_3$ were included, while smaller $CaCO_3$ or those not fully blocking the microchip depth were excluded. The calculated porosity from this method is slightly lower than the actual value (see Figure S2).

Experimental procedure for high-pressure CO_2 injection

After the MICP process, the microfluidic device was disconnected and treated with a weak acid to clear any clogs in the injection and production ports. After reconnection, approximately 10 pore volumes (PVs) of 1.12 mmol/L $CaCl_2$ solution were injected into the pore network to flush out residual weak acid and bacterial solutions. The pore network was then pressurized to the operating range (100–120 barg) by injecting brine at a rate of 50 µL/min against a back pressure regulator.

In the carbonated water injection experiment shown in Figure 3a, carbonated water (pH = 3.11) was prepared by mixing CO_2 with distilled water at 120 barg and room temperature, then equilibrated in a PEEK accumulator for seven days. It was injected into the calcite-functionalized micromodel at the flowrate of 1 µL/min at 100 bar and 32 °C until all carbonate crystals dissolved. The acidic solution reacted with the $CaCO_3$ precipitates, initiating dissolution and forming bicarbonate ions (HCO_3^-), which raised the local pH and slowed further dissolution. Complete dissolution was achieved within 2 hours.

In the supercritical CO_2 injection experiment (Figure 3b), $scCO_2$ was injected into the calcite-functionalized micromodel at a flow rate of 1 µL/min, with the system saturated with water at 120 bar and 35 °C. The CO_2 injection disrupted the natural geochemical equilibrium by increasing CO_2 partial pressure and lowering the pH of the water, initiating the dissolution of $CaCO_3$ precipitates. The formation of CO_3^{2-} from carbonate dissolution raised the aqueous phase pH, triggering secondary

carbonate precipitation. CO_2 exsolution was observed when the CO_2 concentration exceeded its solubility limit, leading to the release of a free CO_2 phase from the supersaturated aqueous phase.

Experimental procedure for microbial interactions during underground hydrogen storage.

After clear clogs in the injection and production ports, approximately 40 PVs of deionized water were injected at 20 µL/min to clean the pore network. *Oleidesulfovibrio alaskensis* was cultured in modified DSMZ growth media (pH 7.1–7.4) supplemented with 21.1 mM Na-lactate and 20 mM Na-acetate [2]. This bacterial suspension was then inoculated into the calcite-functionalized micromodel at 37 ± 0.5°C and 10.55 barg, followed by an 18-hour shut-in period. Hydrogen was injected at 5 µL/min until gas breakthrough was detected at the outlet, followed by 100 PVs of hydrogen injection at the same rate. After drainage, the system was sealed for 7 days, and the spatiotemporal distribution of hydrogen gas and changes in $CaCO_3$ precipitates within the pore network were visualized using a high-resolution microscope. A baseline experiment, using sterile solutions (without microbial cells), was conducted following the same protocol.

The interaction between hydrogen gas and calcite was studied at pressures ranging from 10 to 100 barg. Hydrogen was injected into the water-saturated, calcite-functionalized micromodel at 30°C and a flow rate of 5 µL/min. Similar to the microbial experiments, after gas breakthrough, 100 PVs of hydrogen were injected, and the system was sealed for 7 days to observe changes in hydrogen gas distribution and calcite crystals within the pore network. Experiments were conducted at pressures of 10, 30, 50, and 100 barg.

Supplementary Figures

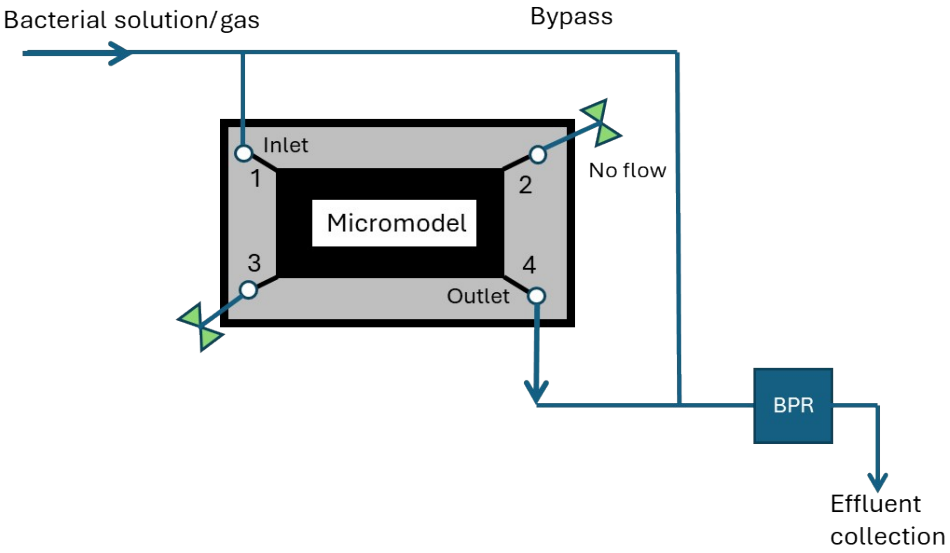

Figure S1. A simplified schematic of the experimental setup illustrates the intended flow into the pore network.

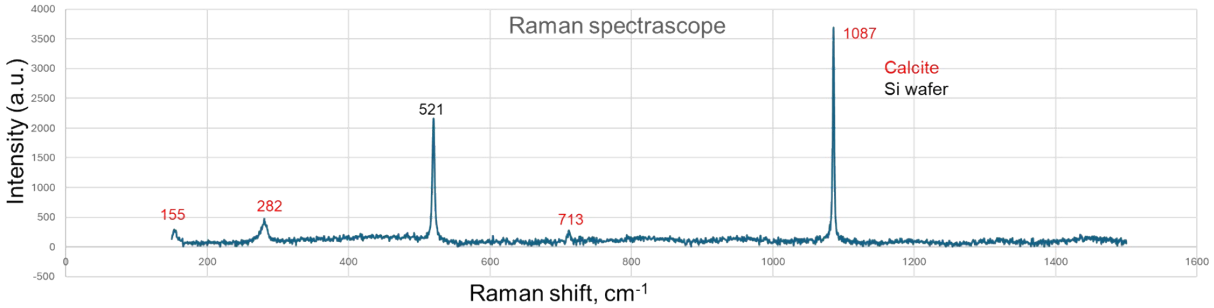

Figure S2. Raman spectra of the $CaCO_3$ precipitates showing the presence of calcite (red peaks) and a silicon signal at 521 cm^{-1}, attributed to the silicon micromodel.

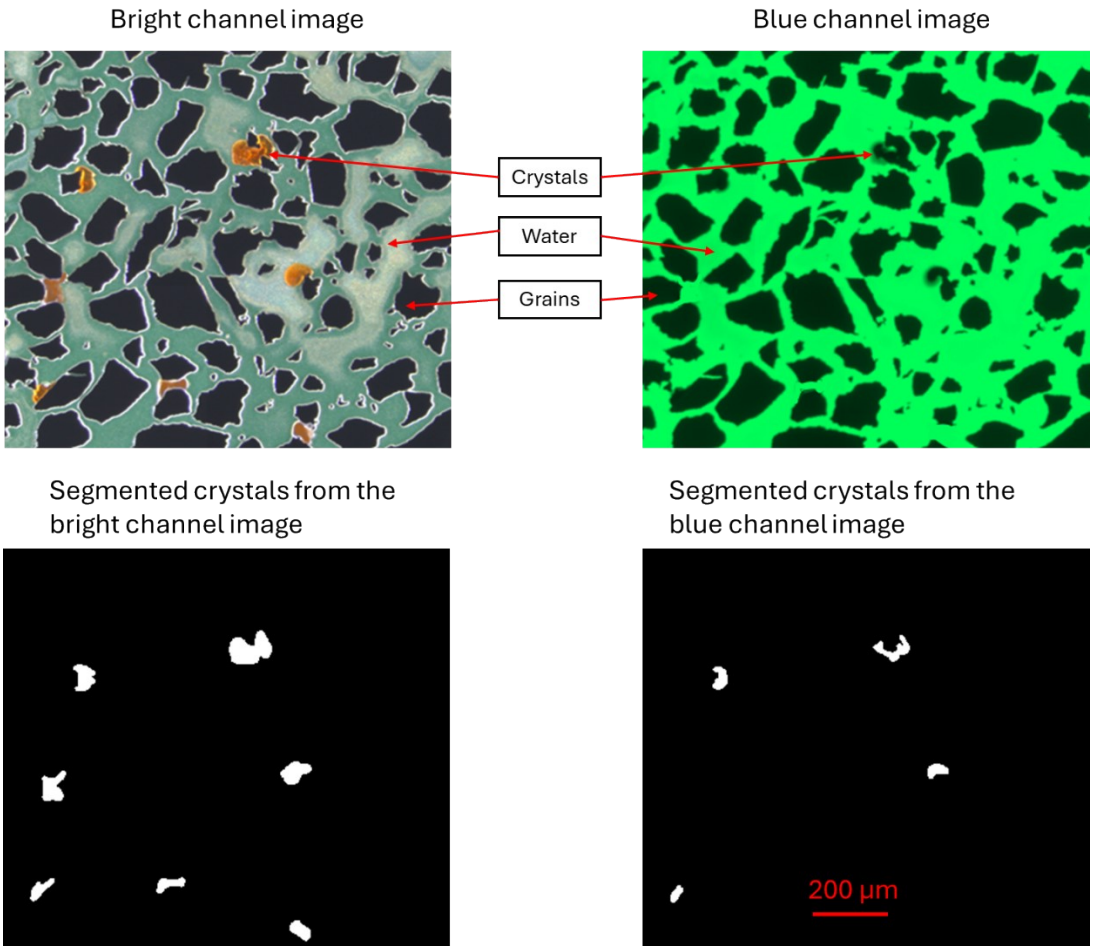

Figure S3. $CaCO_3$ crystals segmentation from bright and blue channel images. Top row: Microscope images captured in the bright field view (left) and the fluorescent view (right). **Bottom row**: Segmented crystal images derived from the top images. In the bright channel, crystals appear brown due to dye and are segmented via color extraction. In the blue channel, only vertically fully grown crystals that block fluorescent water appear as black, resulting in fewer segmented crystals compared to the bright channel.

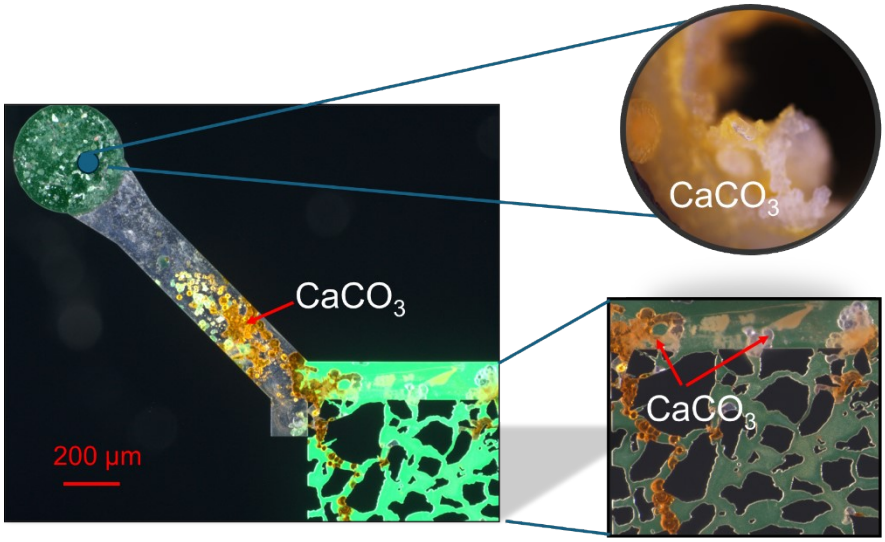

Figure S4. Microscopic images of $CaCO_3$ growth obstructing the connecting tubing and inlet areas. During cementation solution injection, $CaCO_3$ formation rapidly clogged the narrow inlet tube (200 µm width), blocking the entrance. To continue the process, the microchip was disconnected from the setup and immersed in a 0.1 M HCl solution to dissolve the blockage.

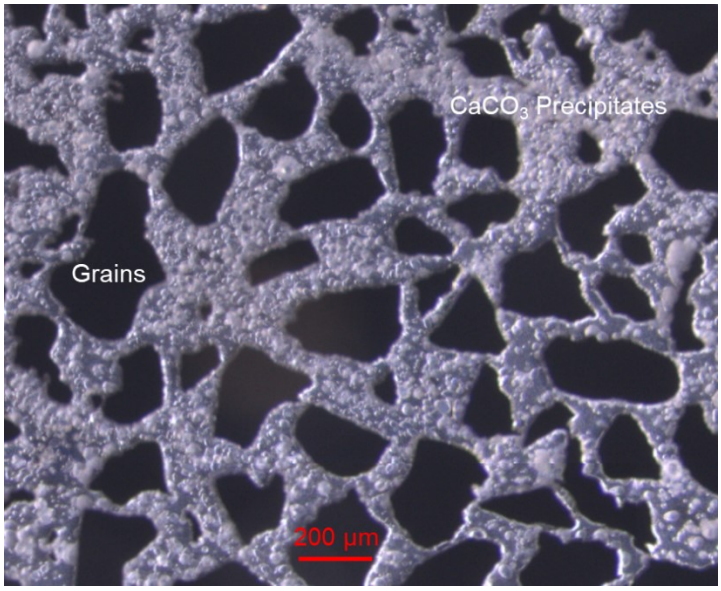

Figure S5. Chemical deposit of $CaCO_3$ in the pore network. This image shows $CaCO_3$ precipitates in the inlet area formed from the chemical deposition of $CaCl_2$ and Na_2CO_3 solutions in the micromodel at ambient conditions. A 0.5 M $CaCl_2$ solution was injected into the pore network at a flow rate of 1 µl/min. Once the pore network was saturated with Ca^{2+}, a 0.5 M Na_2CO_3 solution was introduced at the same rate. The precipitation process occurred rapidly, leading to clogging of the inlet area after approximately 0.5 PVs of CO_3^{2-} solution. The injection channel became quickly obstructed by nanoscale or small-sized (a few micrometers) precipitates, which aggregated and blocked the inlet area.

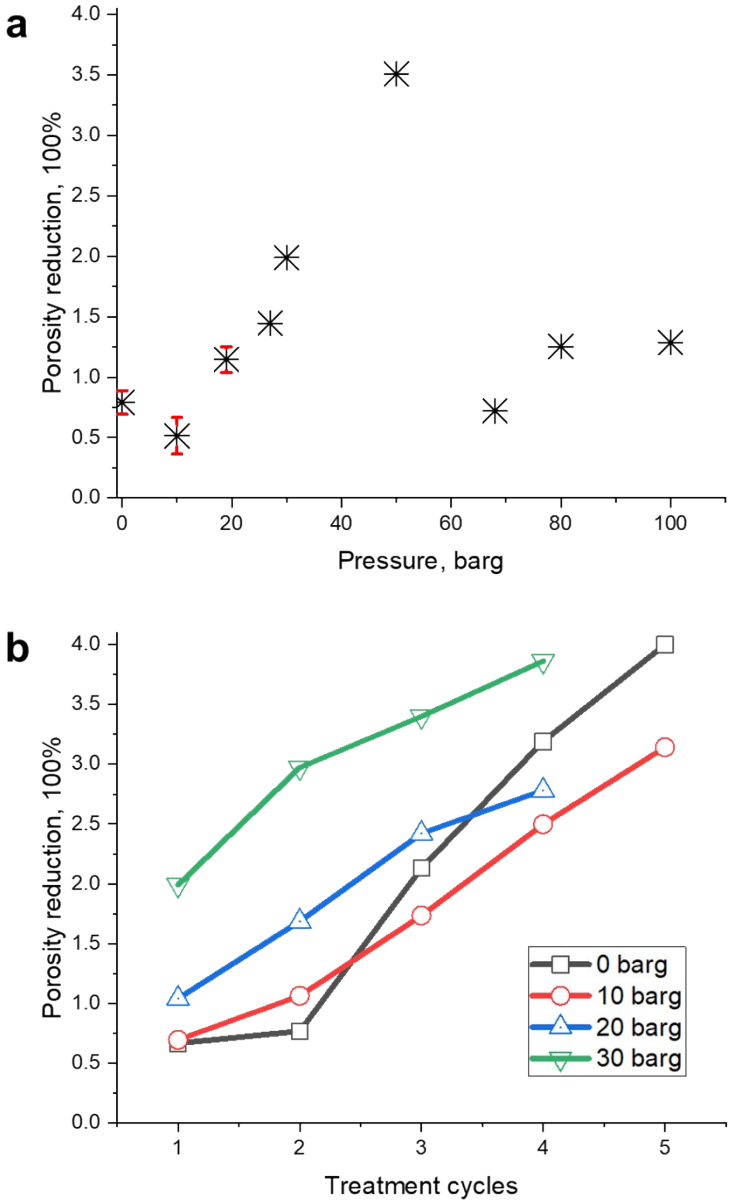

Figure S6. (a), The impact of pressure on porosity during a single cycle shows that porosity decreases as pore pressure increases. This is because higher pressure aids in the dehydration of ACC, promoting calcite (or vaterite) crystallization. As pressure increases, crystal size grows, but the number of crystals decreases. When the pressure exceeds 60 barg, only a few large crystals form, even when using the same injection protocol. A rapid increase in pressure during bacterial inoculation significantly reduces microbial activity, which in turn decreases production and slows urea hydrolysis. As a result, the formation of $CaCO_3$ precipitates dramatically decreases in experiments conducted at pressures above 60 barg. (b), The effects of treatment cycles on porosity were analyzed using data from four experiments conducted at pressures ranging from 0 to 30 barg. At all pressures, porosity decreased linearly with treatment cycles.

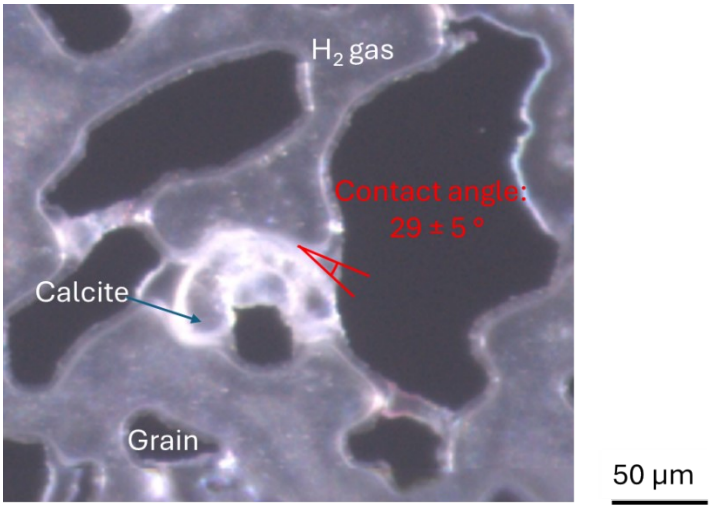

Figure S7. Contact angle of hydrogen gas on the calcite surface. The wettability of the calcite precipitates was assessed by measuring the contact angle in a three-phase system (H_2 gas-water-grains). The contact angle (θ) was quantified using image analysis with the open-source ImageJ software. The measured contact angle ranged from 24.4° to 34.1°, demonstrating the hydrophilic nature of the formed calcite precipitates.

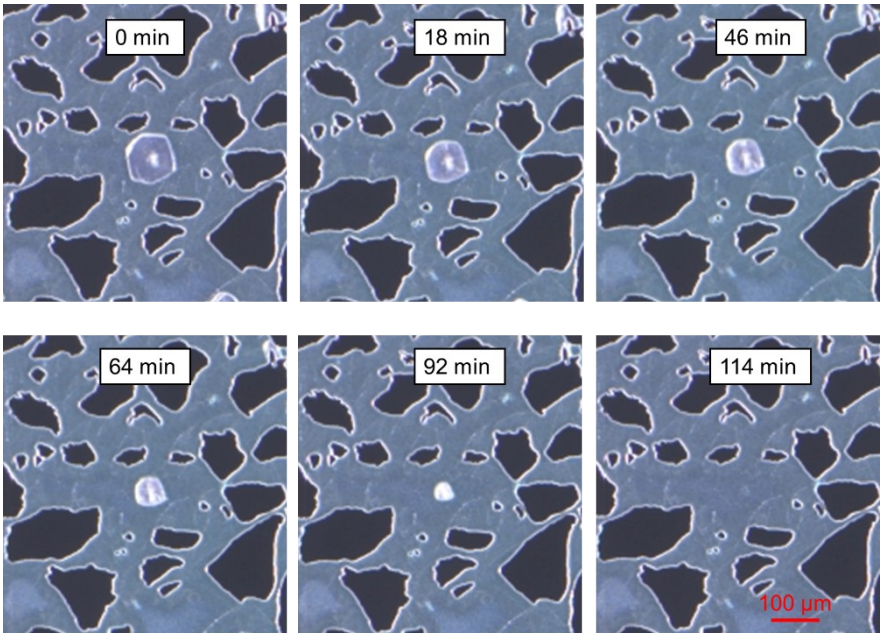

Figure S8. Time-series images of calcite crystal dissolution in carbonated water.

References:

1. N. Liu, M. Haugen, B. Benali, D. Landa-Marbán and M. A. Fernø, *Chemical Geology*, 2023, **641**, 121782.
2. N. Liu, A. R. Kovscek, M. A. Fernø and N. Dopffel, *Frontiers in Energy Research*, 2023, **11**.
3. M. Lysyy, N. Liu, D. Landa-Marbán, G. Ersland and M. Fernø, *Journal of Energy Storage*, 2024, **87**, 111439.
4. B. Benali, A. Sæle, N. Liu, M. A. Fernø and Z. P. Alcorn, *Transport in Porous Media*, 2023, **150**, 427-445.